



Cite this: RSC Adv., 2015, 5, 89869

Dietary flavone chrysins (5,7-dihydroxyflavone ChR) functionalized highly-stable metal nanoformulations for improved anticancer applications†

G. Sathishkumar,^a Rashmi Bharti,^b Pradeep K. Jha,^b M. Selvakumar,^c Goutam Dey,^b Rakhi Jha,^b M. Jeyaraj,^d Mahitosh Mandal^b and S. Sivaramakrishnan*^a

Nanomaterials of noble metals with unique size, shape and composition receives much attention owing to their versatile functionality in personalized cancer nanomedicine. Chrysins (ChR), a natural anticancer bioflavonoid, emerged as a potential drug therapy for almost all types of cancer, however it has poor solubility and bioavailability. Herein, we report a new approach to formulate biofunctionalized metallic silver (ChR–AgNPs) and gold (ChR–AuNPs) nanoparticles using ChR as a direct bioreductant and capping agent. Size and dispersity of nanoparticles (NPs) were controlled through fixing different reaction conditions such as the temperature, pH, concentration of metal ion, stoichiometric proportion of the reaction mixture and incubation time based on their optical properties and SPR effect in UV-visible spectroscopy. The role of hydroxyl and carbonyl groups in functionalizing the metal ions with ChR was confirmed with Fourier transform infrared spectroscopy (FTIR) and X-ray photoelectron spectroscopy (XPS) analysis. It was also substantiated that the oxygen group from ChR donates electrons to metal ion and results in complexation; ionic Ag⁺ and Au³⁺ were reduced to Ag⁰ and Au⁰ nano-forms. The physiochemical state of obtained NPs was characterized through different exclusive instrumentation, which shows the presence of highly-stable, spherical, crystalline ChR–AgNPs and ChR–AuNPs with an average size of 14 ± 6 nm and 6 ± 2 nm respectively. *In vitro* anticancer results revealed that the formulated metallic NPs exhibit enhanced cytotoxicity over ChR in the treatment of two different breast carcinoma cell lines (MDA-MB-231 and MDA-MB-468). Furthermore, it was evident that the NPs cause cell death via the induction of apoptosis. A hemolysis assay with human erythrocytes demonstrates good blood biocompatibility of the NPs. Thus, the ChR functionalized metal NPs can be potentially employed as a combinational drug-nano platform for breast cancer therapy.

Received 29th July 2015
Accepted 28th September 2015

DOI: 10.1039/c5ra15060d
www.rsc.org/advances

1. Introduction

Nano-biotechnology is a constantly fast growing research field at the present time which combines biotechnology, nanotechnology, material science, chemical processing and system engineering. It is actively engaged in the tailoring of new functional nanomaterials with a 10⁻⁹ meter dimension for

various industrial and biomedical applications. Interestingly, these dynamic nanomaterials acquire inimitable size, shape and surface properties compared to their macroscale counterparts.¹ Recently, huge attention was given to the green synthesis of metal nanoparticles through exploiting different biological entities like bacteria,² fungi,³ actinomycetes,⁴ yeast,⁵ algae⁶ and plants.⁷ By virtue of its facile, eco-friendly and cost-effective properties biogenesis was fixed to be the most preferred route over other conventional methods.⁸ Many studies have demonstrated that active metabolites such as polyphenols,⁹ reducing sugars¹⁰ and proteins^{11,12} were found to play a key role in the reduction and stabilization of nanoparticles (NPs). The interaction of biomolecules with nanomaterials will offer new and improved end products. Although biogenic nanomaterials were found to be an effective contrivance, the actual reduction mechanism and how to get a narrow size distribution were yet to be clarified.

^aDepartment of Biotechnology and Genetic Engineering, Bharathidasan University, Tiruchirappalli-620024, Tamilnadu, India. E-mail: sivaramakrishnan123@yahoo.com; Fax: +91-431-2407045; Tel: +91-431-2407086

^bSchool of Medical Science & Technology, Indian Institute of Technology (IIT), Kharagpur-721302, West Bengal, India

^cRubber Technology Centre, Indian Institute of Technology (IIT), Kharagpur-721302, West Bengal, India

^dNational Centre for Nanosciences and Nanotechnology, University of Madras, Guindy Campus, Chennai 600025, Tamilnadu, India

† Electronic supplementary information (ESI) available. See DOI:
10.1039/c5ra15060d

Over the past decade cancer continues to be a huge burden for mankind, despite the existence of diverse therapeutic strategies. Especially, breast cancer is the most common malignancy among women, and incidence rates vary between countries with respect to geography, economic background, life style, age, stage at presentation and biological characteristics.¹³ The occurrence of newer breast cancer cases will show a two fold increase by the end of 2020.¹⁴ The early detection and treatment of cancer has been restricted by dose-limiting systemic toxicity, the prevalence of multiple drug resistance (MDR) and a lack of innovative approaches.¹⁵ To overcome these barriers in cancer therapy, recent cutting edge research has been focused on exploring novel therapeutic modalities to combat breast cancer progression. Numerous dietary antioxidants like catechin, gallicatechin epicatechin-3-gallate, epigallocatechin-3-gallate, apigenin, genistein, glycitein, biochanin A, formononetin, quercetin, kaempferol, myricetin, delphinidin, malvidin and pelargonidin were explored for cancer prevention.¹⁶ Chrysanthemic acid (5,7-dihydroxyflavone) is a natural bioactive dietary flavone abundantly found in honey, passion flowers, *Oroxylum indicum* and propolis. It owns stupendous medicinal properties such as anticancer, anti-inflammatory, antioxidant, hepatoprotective, antimicrobial and anti-diabetic effects. Also, it is now well established that ChR inhibits cancer cell growth through the induction of apoptosis, cell cycle arrest, the inhibition of angiogenesis, invasion and metastasis without adverse side effects on normal cells.¹⁷ While ChR was proposed to be an extraordinary chemotherapeutic agent, it always suffers with a lot of efficacy limitations like poor solubility and bioavailability.¹⁸ An ideal nanoparticulate system of noble metals, polymers and other inorganic materials can improve the target-specificity, porosity and solubility, and increase the bioavailability of various chemotherapeutic agents.¹⁹

The large surface area to volume ratio and different structural properties of nano-drugs will target tumour sites by a passive process. Also, the arrangement of leaky vasculature and poor lymphatic drainage of cancer cells will lead to an enhanced permeability and retention (EPR) effect. Materials at the nanoscale level can easily pass through cellular barriers and strongly interact with functional biomolecules.²⁰ Ultimately, they will offer many biomedical insights for clinical level applications.

Metal NPs such as gold, silver, copper, platinum, palladium, iron, zinc and titanium have gained colossal attention due to their indispensable applications in drug delivery,²¹ imaging,²² and Surface-Enhanced Raman Scattering (SERS) detection,²³ as antioxidants,²⁴ anti-inflammatories,²⁵ and bactericides²⁶ and in cancer theranostics.²⁷ Metal-flavonoid complexes have elicited great interest in recent years for their potential therapeutic applications. In an attempt to further improve the anticancer efficacy of ChR, we have used this flavone as an instant reductant to generate functionalized highly-stable AgNPs and AuNPs. Most importantly it reveals the reduction mechanism and kinetics of the biogenesis of nanomaterials (Scheme 1). On the other hand, *in vitro* anticancer studies demonstrate the enhanced chemotherapeutic potential of formulated NPs for breast cancer therapy.

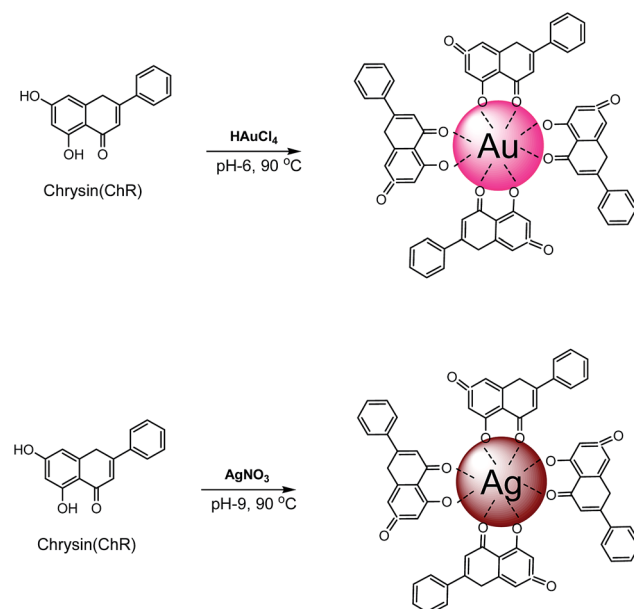
2. Experimental section

2.1. Materials

Silver nitrate (AgNO_3), chloroauric acid (HAuCl_4), chrysanthemic acid (ChR), 3-(4,5-dimethyl-2-thiazolyl)-2,5-diphenyl-2H-tetrazolium bromide (MTT), heat inactivated fetal bovine serum (FBS), minimum essential medium (MEM), glutamine, EDTA and trypsin were purchased from Sigma-Aldrich (St. Louis, USA). All glassware was washed with distilled water followed by acetone and dried in an oven before use. The breast cancer cell lines MDA-MB-231 and MDA-MB-468 were obtained from the National Centre for Cell Science (NCCS), Pune, India.

2.2. Size controlled synthesis of ChR-AgNPs and ChR-AuNPs

In a typical synthesis process, the reaction mixture was prepared by adding 12 mg of ChR to 100 mL of metal ion (1 mmol L⁻¹) solution under constant stirring. The pH was adjusted with 0.1 N NaOH and 0.1 N HCl to reach different pH values ranging from 5–10. The temperature was controlled using a thermostat magnetic stirrer (37 °C, 50 °C, 60 °C, 70 °C, 80 °C, 90 °C and 100 °C). The concentration of the metal ions AgNO_3 & HAuCl_4 (0.5, 1, 1.5, 2 and 3 mM), concentration of ChR (0.5, 1, 1.5 and 2 mM), stoichiometric proportion of metal ion/ChR (1 : 1, 1 : 2, 1 : 3, 1 : 4 and 2 : 1) and incubation time (0–60 minutes) were fixed. Optimal conditions will get control over the nucleation and growth of the NPs with a better size distribution. Influence of these parameters on the size, shape and yield of NPs was studied preliminarily through SPR absorbance spectra using a UV-visible spectrometer.



Scheme 1 Illustration of the reduction and functionalization of AgNPs and AuNPs using chrysanthemic acid (ChR) as a direct bioreductant.

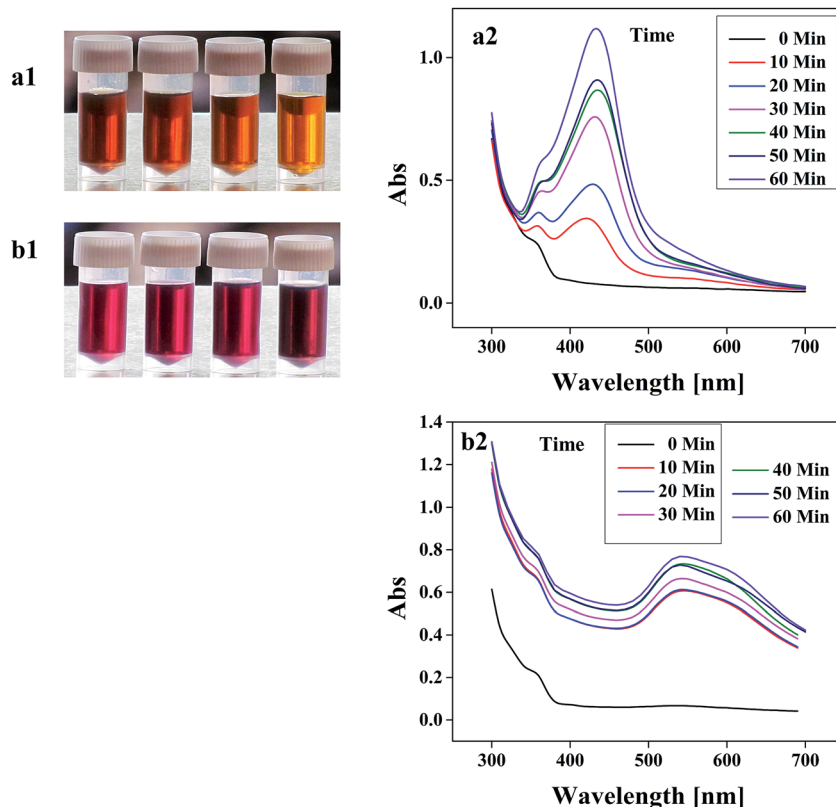


Fig. 1 Color intensity pattern of (a1) ChR–AgNPs and (b1) ChR–AuNPs synthesized at different concentrations of ChR from 0.5 mM to 2 mM; the formation of a yellowish brown color and ruby red color due to excitation of SPR indicates the generation of ChR–AgNPs and ChR–AuNPs respectively. (a2) & (b2) shows the absorbance UV-Vis spectroscopy analysis of ChR–AgNPs and ChR–AuNPs which displays an intense SPR peak at 420 nm and 530 nm.

2.3. Characterization of ChR–AgNPs and ChR–AuNPs

The reduction of AgNO_3 and HAuCl_4 was monitored with a UV-visible spectrophotometer based on the SPR of all the reaction parameters. Before high throughput characterization the colloidal NP suspensions were purified by dialysis using a cellulose tube (MW cutoff 12 400 Da) against 1 L of deionized water for 24 h at 30 °C to remove excess metal ions and unreacted ChR. To perform UV-Vis, a small aliquot of the sample was diluted with distilled water and the absorbance maxima were scanned by a Perkin-Elmer Lambda 2 UV198 UV-visible spectrophotometer, at wavelengths of 300–700 nm. FTIR spectroscopic measurements were carried out to study the surface chemistry of the NPs; samples were mixed with KBr powder and pelletized after drying and the transmittance was recorded using a JASCO 460 PLUS FTIR spectrometer (wavelength range between 4000 cm^{-1} and 400 cm^{-1}). X-ray diffraction (XRD) was performed to determine the dimensions of the synthesized NPs with h , k , l values. The diffraction pattern was obtained with conditions of 40 kV and 30 mA with $\text{Cu K}\alpha$ radiation and the mean particle sizes (L) (PAN analytical X pert PRO Model) of the NPs were calculated using the Debye-Scherrer equation.

$$L = 0.9\lambda/\beta \cos \theta$$

where, λ is the wavelength of the X-rays, β is the full width at half maximum and θ is the Bragg's angle. The surface oxidation state and the presence of elements in the sample were studied using XPS. It was carried out using an omicron ESCA spectrometer with monochromatized $\text{Al K}\alpha$ radiation. Morphology of the nanoparticles was studied using the images obtained with a high resolution transmission electron microscope (HRTEM). To perform the HRTEM analysis, a purified NP solution was allowed for sonication up to 10–20 min, and a drop of this solution was used to make a thin layer on a copper coated grid and allowed to dry. The micrographs were taken at different magnification using a JEOL JEM 2100 HRTEM operating at 100 keV. Energy-dispersive X-ray spectroscopy (EDS or EDX or EDAX) is an analytical technique used for elemental analysis or the chemical characterization of a sample. EDX spectra and selected area diffraction (SAED) patterns of the NPs were obtained along with the HRTEM (JEOL JEM 2100) analysis. The size distribution and surface charge of the synthesized NPs were measured using dynamic light scattering (DLS) and a zeta potential analyzer (Malvern Zetasizer, Nano-ZS90). Concentrations of the formulated NPs were measured with inductively coupled plasma atomic emission spectroscopy (ICP-OES Perkin-Elmer Optima 5300 DV model).

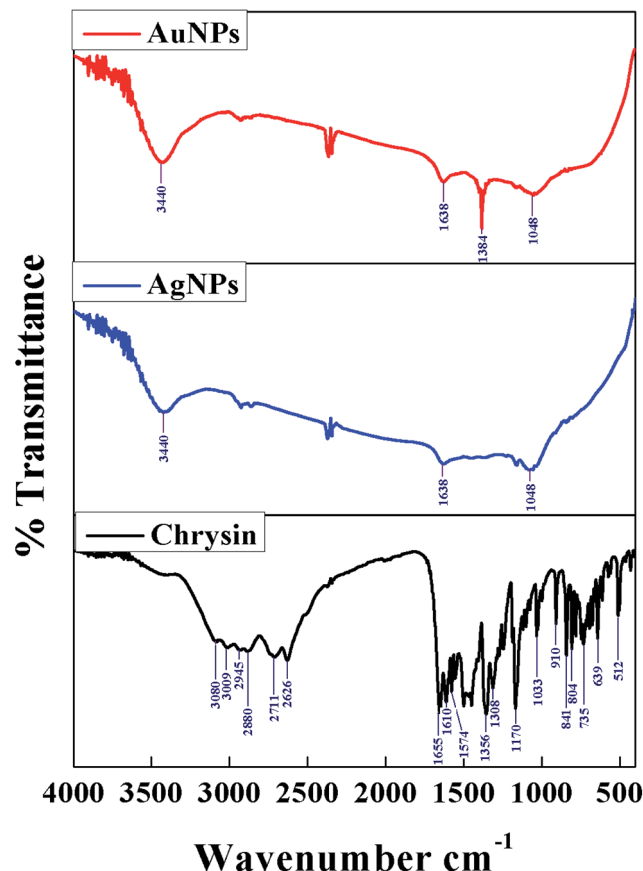


Fig. 2 FTIR transmittance shows the surface absorption of ChR by the metal ions, it strongly confirms the role of hydroxyl ($\text{O}-\text{H}$) and carbonyl ($\text{C}=\text{O}$) functional groups of ChR in the reduction and stabilization of NPs.

2.4. *In vitro* anticancer studies

2.4.1. Cell lines. The MDA-MB-468 and MDA-MB-231 cells were cultured in Dulbecco's Modified Eagle's Medium: Nutrient Mixture F-12 (Ham) (D-MEM/F-12) with 15 mM HEPES buffer, L-glutamine, and pyridoxine hydrochloride, supplemented with 1.2 g of sodium bicarbonate (Invitrogen Corporation, CA), antibiotics (10 000 U L^{-1} penicillin and 10 mg L^{-1} streptomycin) (Himedia, Mumbai, Maharashtra India) and 10% fetal bovine serum (FBS) (Invitrogen, Grand Island, NY, USA). The cells were incubated at 37 °C in a 5% CO_2 and 95% humidified incubator.

2.4.2. Cell viability analysis (MTT assay). The cytotoxicity of the NPs was measured using an MTT (3-(4,5-dimethylthiazol-2-yl)-2,5-diphenyl tetrazolium bromide) assay.²⁸ Briefly, the cells in their exponential growth phase were trypsinized and seeded in 96-well flat-bottom culture plates at a density of 1×10^4 cells per well in 100 μL of complete Dulbecco's modified eagle's medium (DMEM). Then, the cells were allowed to adhere and grow for 24 h at 37 °C in the presence of 5% CO_2 . After 24 h, the medium was replaced with 100 μL of fresh incomplete DMEM medium containing different concentrations of ChR (0, 5, 10, 20, 25, 50, 75, 100, 150 and 200 $\mu\text{g mL}^{-1}$), ChR-AgNPs and ChR-AuNPs (0, 2, 5, 10, 15, 20, 25, 30, 40 and 50 $\mu\text{g mL}^{-1}$) and

incubated for 48 h at 37 °C in 5% CO_2 . At the end of the incubation, fresh media containing 0.40 mg mL^{-1} MTT were added to the 96-well plates and they were incubated for another 4 h at 37 °C in 5% CO_2 . The formazan crystals formed after 4 h were solubilized in 100 μL of DMSO after aspirating the medium. The absorbance was monitored at 595 nm using a 96-well plate reader (Bio-Rad, Hercules, CA, USA). The growth inhibition was determined using:

$$\text{Growth inhibition} = (\text{control O.D.} - \text{sample O.D.})/\text{control O.D.}$$

The IC_{50} value was defined as the concentration of NPs that produced a 50% reduction in cell viability.

2.4.3. Analysis of apoptosis (TUNEL assay). The level of apoptosis induced by ChR and the formulated NPs was identified via terminal deoxynucleotidyl transferase (TdT)-mediated dUTP nick end labelling (TUNEL) staining using the *in situ* Cell Death Detection Kit-Fluorescein (Roche Molecular Biochemicals, Chemicon Int., Temecula, CA, USA) as per the manufacturer's instructions. Briefly, the cells were grown on poly-L-lysine-coated glass cover slips and treated with ChR, ChR-AgNPs and ChR-AuNPs for 48 hours. Subsequently, the medium was removed and the slides were washed three times with PBS (pH 7.4), fixed with 4% paraformaldehyde in PBS (pH 7.4) and permeabilized with 0.1% Triton X-100. Aliquots (50 μL) of the reaction mixtures were applied to the cover slides and placed in a humidified incubator at 37 °C for 60 minutes. After incubation, the cells were washed with PBS, air dried and mounted on slides. Finally, the slides were examined by epifluorescence microscopy.²⁹

2.4.4. Hemocompatibility assay. A hemocompatibility assay was performed as per the earlier report³⁰ with slight modification. The sample ChR, ChR-AgNPs and ChR-AuNPs were individually suspended in 10 mM HEPES buffered saline. Fresh blood was collected from healthy volunteers in sterile lithium heparin vacutainers. Red blood cells (RBCs) were separated using centrifugation (1500 rpm for 10 min at 4 °C) and a ficoll density gradient. The RBCs were further diluted in 20 mM HEPES buffered saline (pH 7.4) to form a 5% v/v solution. The RBC suspension was added to HEPES saline, 1% Triton X-100 and samples with different concentrations of ChR (2, 5, 7 and 9 $\mu\text{g mL}^{-1}$), ChR-AgNPs and ChR-AuNPs (10, 20, 30 and 40 $\mu\text{g mL}^{-1}$) and incubated at 37 °C for 30 and 60 min. All the samples were prepared in triplicate and after being slightly vortexed the suspension was incubated under static conditions for 4 h at 37 °C. After incubation, all the samples were centrifuged (Heraeus table top centrifuge 5805R, Germany) at 12 000 rpm at 4 °C and the supernatants were transferred to a 96-well plate. The hemolytic activity was determined by measuring the absorbance at 570 nm (Biorad microplate reader model 550, Japan). Control samples of 0% lysis (in HEPES buffer) and 100% lysis (in 1% Triton X-100) were employed in the experiment. The percent of hemolysis was calculated as follows:

$$\text{Hemolysis\%} = [(\text{sample absorbance} - \text{negative control}) / (\text{positive control} - \text{negative control})] \times 100\%.$$

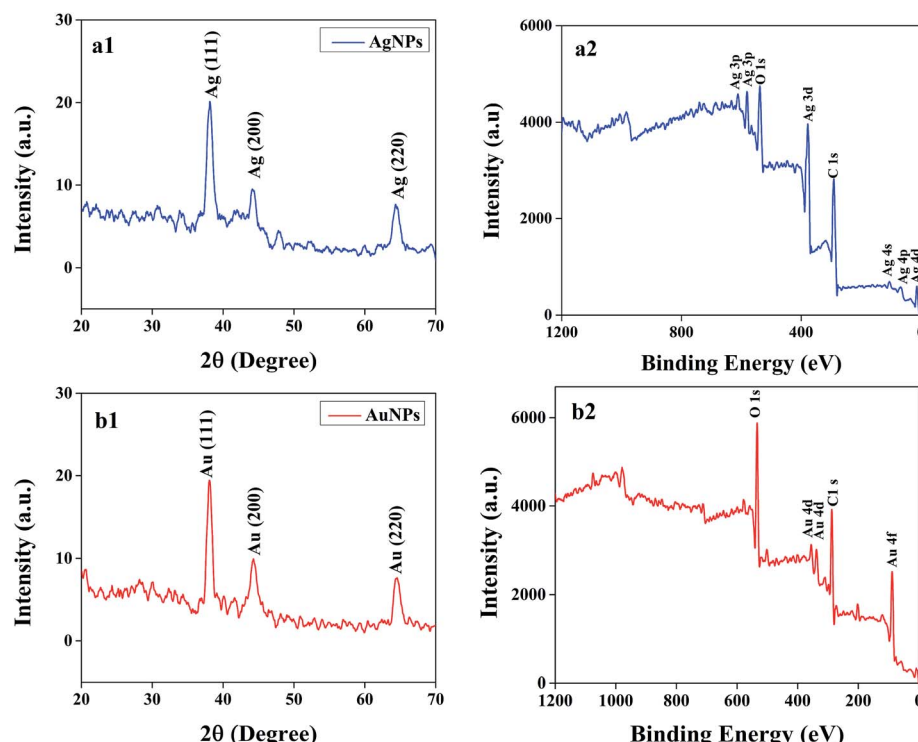


Fig. 3 XRD pattern of synthesized ChR–AgNPs and ChR–AuNPs (a1 & b1) shows the diffraction index for face centered cubic (fcc) silver (Ag) and gold (Au). XPS survey of (a2) ChR–AgNPs and (b2) ChR–AuNPs.

This study was approved by the Institutional Ethics Committee (IEC) of Bharathidasan University (Ref no. DM/2014/101/54). A consent form with all the mandatory information was collected from the healthy volunteers for their participation in this study, and the form was submitted to IEC, Bharathidasan University.

3. Result and discussion

Generation of metallic Ag and Au nanostructures by the reduction of AgNO_3 and HAuCl_4 with chrysanthemum was initially confirmed through the formation of a yellowish brown and ruby red colour respectively. Fig. 1a1 & b1 show a variation in the colour intensity of the ChR–AgNPs and ChR–AuNPs synthesized at different ChR concentrations attributed to the SPR phenomenon, which relies on size, shape and dispersity of the nanoparticles.^{31,32} The preliminary results revealed that ChR can be used as a direct bioreductant to fabricate AgNPs and AuNPs without the addition of any other toxic chemical ingredient.

3.1. Size controlled synthesis of ChR–AgNPs and ChR–AuNPs

As mentioned earlier, after blending ChR with the metal ions the reaction mixture exhibits variations in colour due to the excitation of Surface Plasmon Resonance (SPR); the formation of a yellowish brown colour and ruby red colour indicates the synthesis of the ChR–AgNPs and ChR–AuNPs. The optimal reaction mixture to synthesize monodispersed stable

nanomaterials was fixed at 0.5 mM ChR and 1 mM metal ions in a 1 : 2 ratio (Fig. S1a–c & S2a–c ESI†). The NPs generated at this stoichiometric proportion generate intense SPR spectra which clearly denote the presence of smaller nanoparticles, whereas the other precursor concentrations produce broad and weaker SPR peaks due to increased polydispersity.³³ As per the LaMer model, it was envisaged that the formation of NPs could only happen when the precursor concentration was within a suitable range for nucleation. However, this range might vary amongst different biomass-assisted synthesis approaches. Dubey *et al.* (2010), observed that NPs synthesized at higher metal ion concentrations were larger and a red shift occurred in the SPR spectra as an indication of the polydispersity.³⁴

Likewise, the physiological parameters such as temperature and pH mainly influence the synthesis of NPs. Increasing the temperature (37°C to 100°C) reflects in the nucleation growth of NPs. Synthesis was found to be more successful at 90°C when compared to other temperatures, the ChR–AgNPs and ChR–AuNPs synthesized at 90°C show SPR peaks at 420 nm & 530 nm (Fig. S1d & S2d ESI†). Above 90°C the SPR peak was observed at lower wavelength regions due to the reduced size range of the NPs and they were found to be unstable. It was believed that less successful synthesis of the NPs occurred at lower temperatures because the plasmon band was not accompanied by a significant increase in the intensity at lower temperatures.³⁵ Increasing the temperature reflects in SPR peak; at a higher temperature the rate of NP synthesis reached a maximal point which shows an intense absorbance peak relative to the size of NPs.³⁶

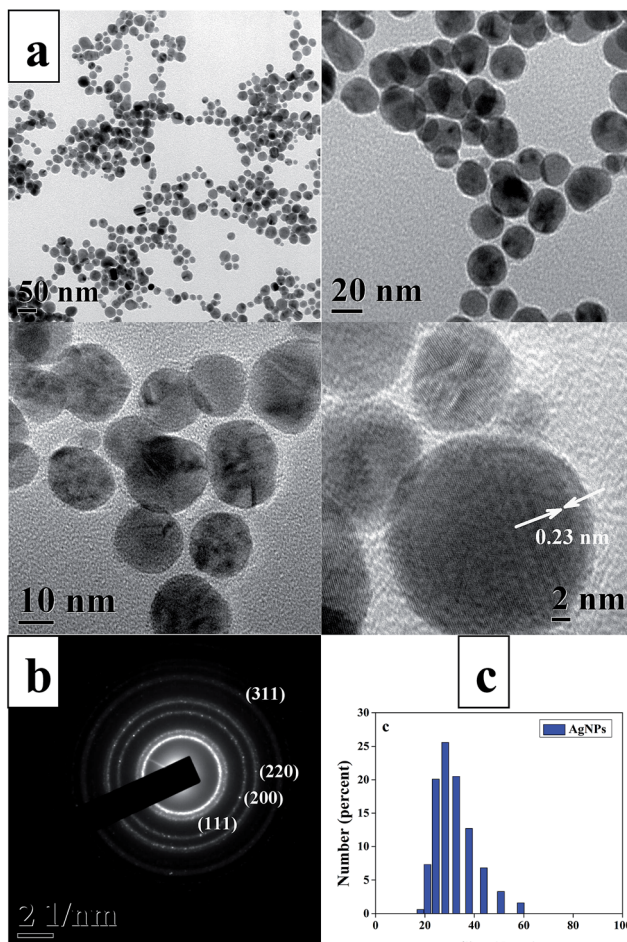


Fig. 4 HRTEM micrographs of ChR–AgNPs (a) showing well dispersed spherical-shaped ChR–AgNPs with an average size of 14 ± 6 nm and high-magnification image of a single nanocrystal showing lattice fringes with a spacing of 0.23 nm, (b) SAED pattern and (c) DLS particle size distribution pattern.

The pH of the reaction medium plays a crucial role in the metal ion reduction, from our results it was inferred that in alkaline pH 9 (Fig. S1e ESI†) the synthesis of ChR–AgNPs was found to be more successful. At an alkaline pH, the aggregation of NPs was believed to be favoured over nucleation to form narrow sized nanoparticles.³⁷ On the other hand, stable ChR–AuNPs were formed at acidic pH 6 (Fig. S2e ESI†), generating an intense SPR peak at 530 nm. Usually, the biosorption mechanism of Au is ionic rather than covalent due to the dependence of Au binding on pH. At lower pH, gold is present in solution in anionic form (AuCl_4^-) and the functional groups of active biocompounds on the biomass surface such as the hydroxyl groups tend to undergo protonation and become positively charged. The overall positively charged surface could promote the interaction between protonated functional groups and negatively charged AuCl_4^- through electrostatic attraction or electrovalent bonding.³⁸ As a result, biosorption was preferred over the bioreduction of Au ions. The bioreduction of gold could occur through the oxidation of hydroxyl to carbonyl groups. The pH of the colloid is lowered in most cases after the synthesis is completed. In our study, the

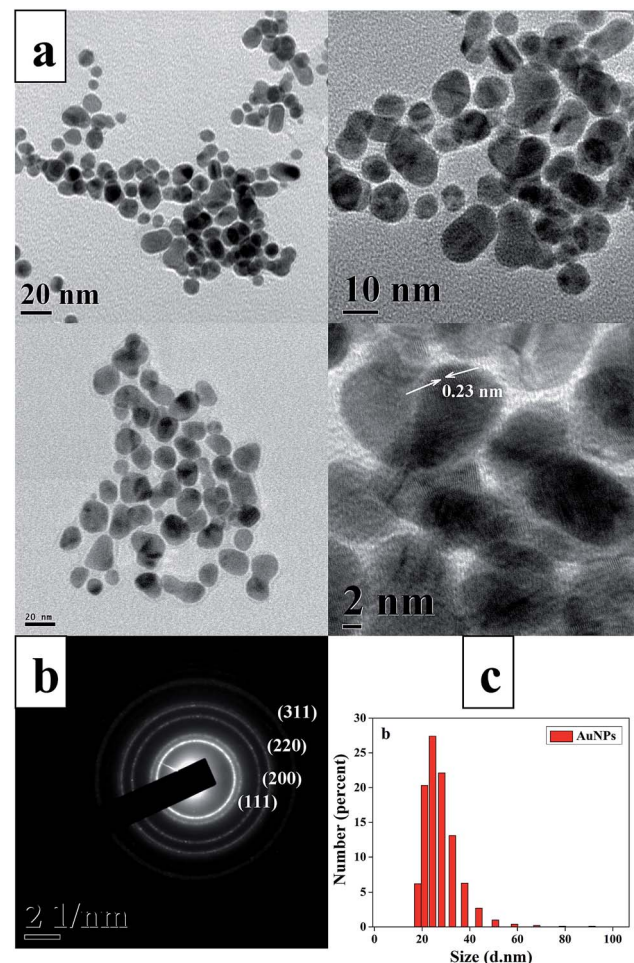


Fig. 5 HRTEM micrographs of ChR–AuNPs (a) showing well dispersed spherical and oval-shaped ChR–AuNPs with an average size of 6 ± 2 nm and high-magnification image of a single nanocrystal showing lattice fringes with a spacing of 0.23 nm, (b) SAED pattern and (c) DLS particle size distribution pattern.

complete reduction of the metal ion was noticed after 60 min incubation time, and the yield of the NPs was directly proportional to the reaction time. Similarly, Dwivedi *et al.* (2010), reported that the peak absorbance was sharper when the contact time was increased to 2 h time duration.³⁹ As compared to previous reports our synthesis method requires much shorter times which can be useful for an easy scaling up process.

3.2. Characterization of ChR–AgNPs and ChR–AuNPs

Generally, noble metal NPs were known to exhibit the SPR phenomenon where the conducting electrons of metals oscillate collectively in resonance to certain wavelengths upon interaction with an electromagnetic field. These SPR bands highly depend on the type, size, and shape of the NPs and their surrounding environment.⁴⁰ UV-visible spectroscopy displays an intense SPR peak at 420 nm for the ChR–AgNPs and 530 nm for the ChR–AuNPs (Fig. 1a2 & b2), and the synthesized NPs were stable at room temperature even after 45 days. The IR spectrum of free ChR manifests prominent transmittance

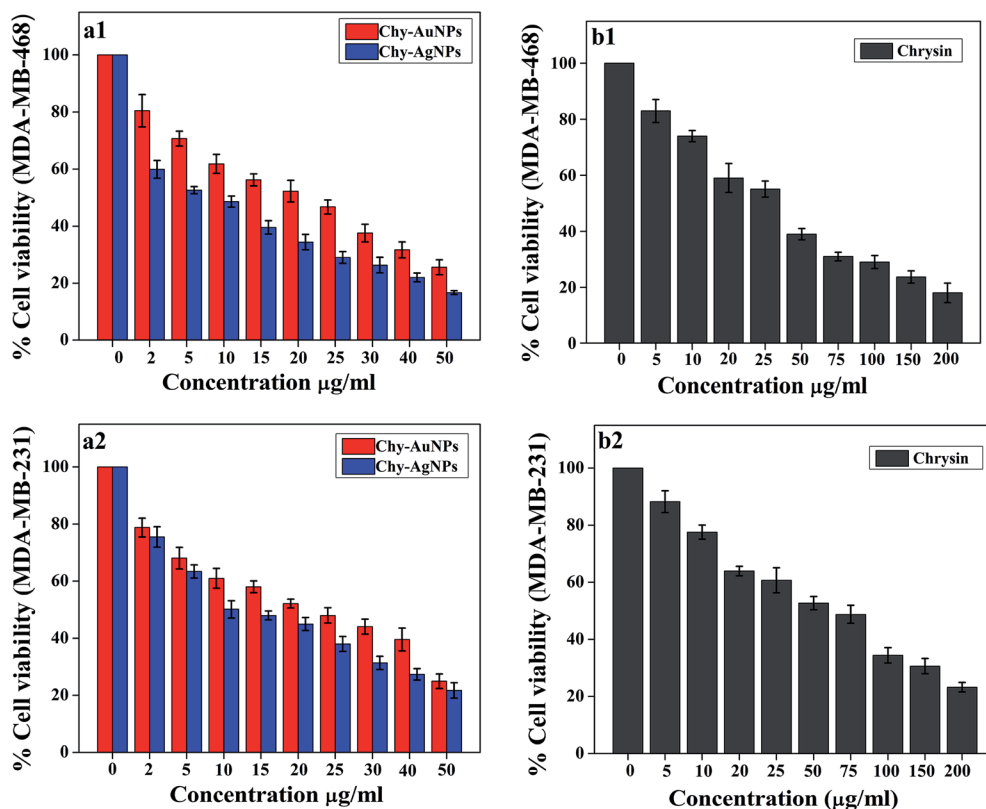


Fig. 6 *In vitro* antiproliferative assay by an MTT reagent in MDA-MB-468 and MDA-MB-231. (a1 and a2) Formulated ChR–AgNPs, ChR–AuNPs and (b1 and b2) free ChR were given at different doses for 48 h. All the data are expressed as the mean \pm SD of the three experiments with duplicate wells.

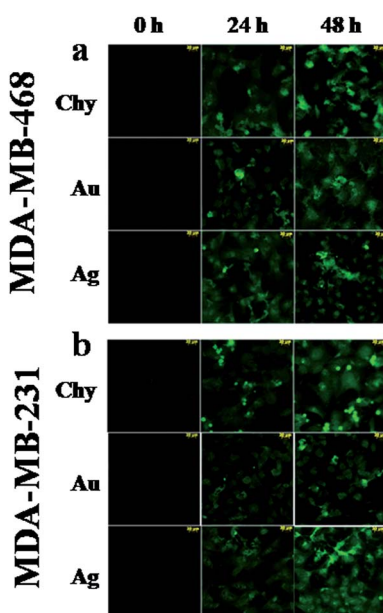


Fig. 7 Induction of apoptosis by formulated Chr-AgNPs, Chr-AuNPs and free Chr was measured through a TUNNEL assay in treated (a) MDA-MB-468 and (b) MDA-MB-231 breast carcinoma cell lines. Epi-fluorescence microscopic image shows apoptotic cells (TUNEL-positive nuclei) at different incubation time intervals (24 h and 48 h).

located at 3080, 3009, 2945, 1655 and 1610 cm^{-1} (Fig. 2). The strong bands between 3500–3000 cm^{-1} correspond to the O–H stretch whereas those at 1655 and 1610 cm^{-1} are attributed to C=O and C=C respectively. The characteristic IR transmittance of synthesized NPs clearly implicates that the functional groups of ChR actively participate in coordination with the metal ions. Variations in the intensity of transmittance at 3500–3000 cm^{-1} are noticed in the formulated ChR-NP complexes which clearly depict that the symmetrical and asymmetrical stretching modes of O–H undergo changes after the reduction. This difference in intensity suggests the loss of one O–H group during the coordination to the metal ions.⁴¹ A strong band at about 1655 cm^{-1} detected in the transmittance of the ligand is assigned to C=O which was shifted to 1638 cm^{-1} in the spectra of the ChR-NP complexes which denotes that the functionalization of ChR on the metal NPs occurs through the C=O oxygen atom.⁴²

The XRD patterns of the ChR–AgNPs and ChR–AuNPs were interpreted with JCPDS intensities; after reduction the diffraction peaks at $2\theta = 38.03^\circ$, 46.18° and 63.43° were indexed as the (1 1 1), (2 0 0) and (2 2 0) planes of a face centered cubic (fcc) lattice of silver (JCPDS, file no. 04-0783) (Fig. 3a1). The XRD patterns displayed here are consistent with earlier reports.⁴³ Likewise, for the AuNPs, the obtained XRD peaks correspond to three peaks (JCPDS, no. 89-3722) at 38.17° , 44.36° and 64.65° (Fig. 3b1) which are found to be an identical with those reported

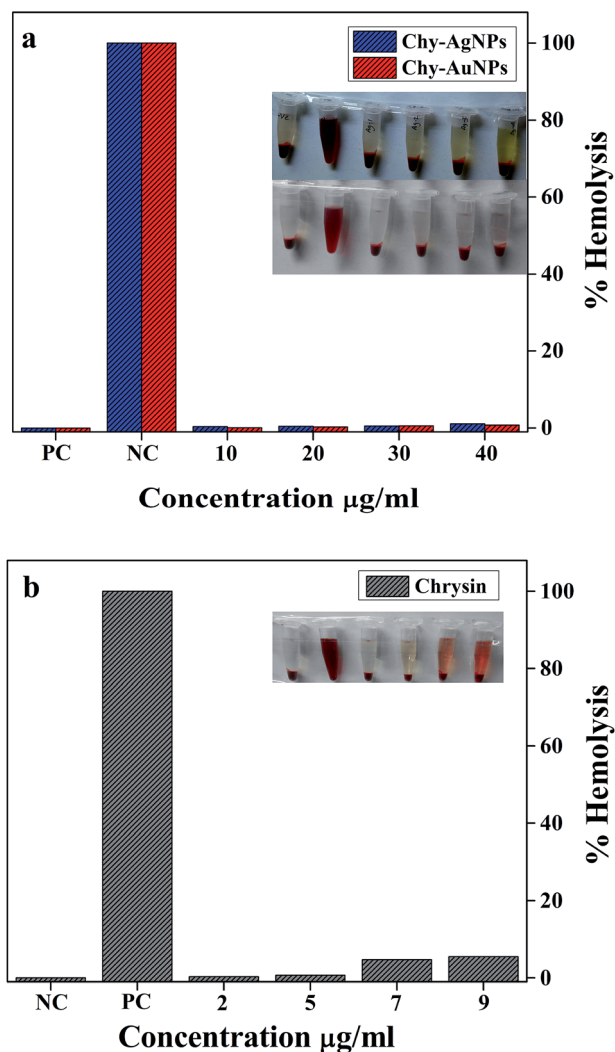


Fig. 8 *In vitro* hemocompatibility assay of (a) formulated ChR–AgNPs and ChR–AuNPs, and (b) free ChR. No (0%) lysis was noticed in the negative control (NC–HEPES buffer) whereas the positive control (PC–1% Triton X-100) shows 100% lysis. Formulated NPs exhibit much less hemolytic activity than free ChR.

for standard gold metal (Au°).⁴⁴ The mean size of the ChR–AgNPs and ChR–AuNPs was calculated using the Debye–Scherer equation by determining the width of the (1 1 1) peak and was found to be 15 and 8 nm respectively which is in fair agreement with the HRTEM measurements.

Fig. 3a2 & b2 display the XPS general scan spectra of ChR–AgNPs and ChR–AuNPs which showing the presence of strong C 1s, O 1s, Ag 3d and Au 4f core levels accordingly. The strong signal of Ag 3d (370 eV) and Au 4f (87.5 eV) indicates the presence of Ag and Au metal. The C 1s peak observed at a binding energy of ~285 eV serves as a reference to correct the binding energy shift of the NPs and it also stems from ChR coordinating. The spectrum also consists of O (~531 eV) elements in their respective binding energy positions due to the interaction of ChR with the synthesized NPs. Thus, it was concluded from the XPS measurements that the metal ions were reduced to a nanometallic form, and the NPs were capped by ChR.^{24,42}

HRTEM micrographs display the fine configuration of uniformly sized spherical ChR–AgNPs with a mean size of 14 ± 6 nm (Fig. 4a). Interestingly, the Au colloid displays both spherical and oval-shaped NPs with an average size of 6 ± 2 nm (Fig. 5a). It was also found that both the ChR–AgNPs and ChR–AuNPs have a thin layer of the ChR coating on their surface, and the particles were well dispersed and stable for a long period of time. No direct contact of the particles was noticed, this is mainly due to the presence of a capping agent.⁴⁵ The higher magnification TEM micrographs expose the excellent crystallinity of NPs, and the distance of 0.23 nm between the lattice planes is in agreement with the (1 1 1) lattice spacing of face centered cubic (fcc) Ag ($d_{111} = 0.2359$ nm) and Au (0.235 nm). The crystalline nature of NPs was further evidenced by SAED patterns (Fig. 4b & 5b). Clear lattice fringes in high-resolution TEM images and the typical SAED patterns (Fig. 4b & 5b) with bright circular rings corresponding to (1 1 1), (2 0 0), (2 2 0), (3 1 1) and (2 2 2) planes indicate that the synthesized NPs are highly crystalline.⁴² EDAX spectra display a strong metal peak for Ag and Au, and the presence of copper is due to the copper grid used for HRTEM-analysis (Fig. S3a & b†). The hydrodynamic diameter of ChR–Ag and AuNPs was evaluated by DLS which confirms the particle size distribution (Fig. 4c & 5c), and the corresponding zeta potential values are suggestive of the high stability of NPs (Fig. S4a & b†). The large negative potential value could be due to the capping agent, which generates repulsive forces between the NPs.⁴⁶ ICP-OES results specify that the concentrations of synthesized NPs were quantified to be 65.89 & 103.3 mg L⁻¹ for the ChR–AgNPs and ChR–AuNPs in that order. It denotes that more than 80% of the metal ions have been reduced to nano scale values.

3.3. *In vitro* anticancer studies

3.3.1. Analysis of cell viability (MTT assay). Cell viability assay clearly explains the cellular response to a toxicant, and in our study the synthesized NPs exhibit higher anticancer activity than ChR. A dose-dependent cellular toxicity was observed for ChR (0, 5, 10, 20, 25, 50, 75, 100, 150 and 200 $\mu\text{g mL}^{-1}$); the synthesized ChR–AgNPs and ChR–AuNPs (0, 5, 10, 20, 30, 40, and 50 $\mu\text{g mL}^{-1}$) treated MDA-MB-468 and MDA-MB-231 breast cancer cell lines. The ChR–AgNPs show a more cytotoxic effect ($\text{IC}_{50} = 15 \mu\text{g mL}^{-1}$ & $12 \mu\text{g mL}^{-1}$) followed by the ChR–AuNPs ($\text{IC}_{50} = 19 \mu\text{g mL}^{-1}$ & $21 \mu\text{g mL}^{-1}$) and ChR ($\text{IC}_{50} = 72 \mu\text{g mL}^{-1}$ & $35 \mu\text{g mL}^{-1}$) against MDA-MB-468 (Fig. 6a1 & b1) and MDA-MB-231 (Fig. 6a2 & b2) breast cancer cell lines. Especially, the cytotoxicity effect of formulated NPs was much stronger than free ChR, which depicts the improved anticancer efficacy of ChR after functionalization with the Ag and Au nanostructures. The size, shape, surface area and surface functionalization of NPs are the major factors that influence the biokinetics and toxicity.⁴⁷ It should be mentioned that the concentration of synthesized NPs used in this case was much less than that of ChR. This decrease in cell viability with an increase in the NP concentration suggests that a greater number of NPs could accumulate inside the cells resulting in enhanced stress, ultimately leading to cell death. These results clearly specify the enhanced effectiveness

of ChR functionalized NPs against cancer cells. It was demonstrated in our earlier study that AgNPs synthesized using the pharmacologically important *Dendrophthoe falcata* with a size range of 5–45 nm have shown enhanced cytotoxicity against human breast carcinoma cells (MCF-7) compared to the aqueous plant extract.³⁷ Similarly, when Selim and Hendi (2012) reported the toxic response of AuNPs to human breast epithelial MCF-7 cells, they noticed the cytotoxic effect of AuNPs on MCF-7 cells and the apoptotic response in a dose dependent manner.⁴⁸

3.3.2. Analysis of apoptosis (TUNEL assay). Apoptosis is the key event in cancer therapy that can be measured with the activation of caspase-cascade, chromatin aggregation, and the partition of cytoplasm and nucleus into membrane-bound vesicles (apoptotic bodies) which contain ribosomes, morphologically intact mitochondria, and nuclear material.⁴⁹ We performed TUNEL staining to identify the apoptotic cell death induced by ChR, and the synthesized ChR-AgNPs and ChR-AuNPs. TUNEL-positive nuclei were found throughout the photomicrographs of treated groups but few were found in the untreated controls, and the numbers of positive nuclei increased with the treatment time (Fig. 7a & b). Previous studies have shown that the possible mechanism involved in the AgNPs induced cellular toxicity begins with the cellular uptake of the inorganic nanoparticles through clathrin-dependent endocytosis and macropinocytosis.⁵⁰

Inorganic NPs profoundly interact with cells and intracellular macromolecules like proteins and DNA.⁵¹ The cellular uptake of the NPs leads to the generation of reactive oxygen species which provokes oxidative stress. It is clearly evidenced that the synthesized NPs (both Ag and Au) induce cell damage through the loss of cell membrane integrity, oxidative stress and apoptosis. Several factors influence the toxicity of NPs such as dose, treatment time and size of the particles and it was found that the biogenic AgNPs and AuNPs show dose and time dependent toxicity against HeLa cells.^{52,53} It was discussed that the biologically synthesized AgNPs cause cellular damage in the Hep-2 cell line through the induction of oxidative stress.⁵⁴ Recently several studies have shown that the AgNPs trigger intracellular ROS by inhibiting the synthesis of intracellular antioxidant systems. The generated ROS favor DNA damage leading to cell death; Piao *et al.*, reported that highly reactive hydroxyl radicals released by AgNPs cause damage to cellular components including DNA.⁵⁵ According to an earlier study, it was documented that AgNPs functionalized with plant phenolics induce oxidative stress that leads to apoptosis via mitochondria-dependent and caspase-mediated pathways.⁵²

3.3.3. Hemocompatibility assay. Hemocompatibility of ChR, and the synthesized ChR-AgNPs and ChR-AuNPs was assessed upon measuring the damage to human RBCs. Our results show that the synthesized NPs exhibit comparatively lower red haemoglobin release than ChR. Fig. 8a & b are photographs of the RBCs exposed to the ChR-AgNPs, the ChR-AuNPs and free ChR at different concentrations. As shown in Fig. 8, compared to the positive control and ChR the haemolytic activity of the NPs was less considerable, implying its safe nature for application. The mechanisms of direct haemolytic activity for different toxic agents were found to be non-specific.

Especially, plant derived xenobiotic compounds such as phenols are capable of promoting haemolysis through the oxidation of haemoglobin, forming metahemoglobin.⁵⁶ Our data highly corroborates the findings of Ruden *et al.*⁵⁷ who reported that silver nanoparticles did not show haemolytic activity against erythrocytes even at higher concentrations (up to 1024 µg mL⁻¹). In another report, AuNPs synthesized using *Z. officinale* extract have shown high level compatibility with blood cells and do not initiate any aggregation of cells, and also the NPs do not seem to activate the platelets. It was inferred that the surface passivation of nanomaterials with different bioagents will improve their biocompatibility.⁵⁸ Eventually, this can be easily used for different biological applications, which require them as vehicles for drug release. Moreover, as per the International Organization for Standardization Technical Report 7406, the haemolysis admissible level of bio-based materials was 5%. The exposure of ChR functionalized metallic nanomaterials shows a meagre level of haemolysis, revealing their biocompatibility and suitability for biomedical applications.

4. Conclusions

A natural anticancer flavone ChR (5,7-dihydroxyflavone ChR) has been used to synthesize AgNPs and AuNPs *via* a greener route without toxic additives. ChR strongly reduces Ag⁺ and Au³⁺ into their nano-forms with a uniform size, shape and surface chemistry. The size and dispersity of nanoparticles were controlled by changing the different reaction conditions. It was observed that the metal ions strongly absorb ChR *via* the hydroxyl group and are functionalized for improved stability. The formulated NPs have shown tremendous anticancer activity against breast carcinoma cells; the NPs trigger cellular toxicity *via* apoptosis. Compared to free ChR the synthesized NPs give improved anticancer action, depicting the enhanced solubility, bioavailability and durability of ChR after functionalization with the NPs. In contrast, ChR capped NPs show less haemolytic activity than ChR, portraying their biocompatible nature. This opens up several possibilities for the ChR-NPs to be used as an appropriate therapeutic approach to save a breast cancer patient's life. Further studies are in progress to implicate the molecular mechanism and metabolic pathways involved in cellular apoptosis.

References

- J. Huang, Q. Li, D. Sun, Y. Lu, Y. Su, X. Yang, H. Wang, Y. Wang, W. Shao, N. He, J. Hong and C. Chen, *Nanotechnology*, 2007, **18**, 1.
- T. Klaus, R. Joerger, E. Olsson and C. Granqvist, *Proc. Natl. Acad. Sci. U. S. A.*, 1999, **96**, 13611.
- P. Mukherjee, A. Ahmad, D. Mandal, S. Senapati, S. R. Sainkar, M. I. Khan, R. Ramani, R. Parischa, P. V. Ajayakumar, M. Alam, M. Sastry and R. Kumar, *Angew. Chem., Int. Ed.*, 2001, **40**, 3585.
- A. Ahmad, S. Senapati, M. I. Khan, R. Kumar and M. Sastry, *Langmuir*, 2003, **19**, 3550.

- 5 M. Kowshik, S. Ashtaputre, S. Kharrazi, W. Vogel, J. Urban, S. K. Kulkarni and K. M. Paknikar, *Nanotechnology*, 2003, **14**, 95.
- 6 J. Xie, J. Y. Lee, D. I. C. Wang and Y. P. Ting, *ACS Nano*, 2007, **1**, 429.
- 7 G. Sathishkumar, C. Gobinath, K. Karpagam, V. Hemamalini, K. Premkumar and S. Sivaramakrishnan, *Colloids Surf., B*, 2012, **95**, 235.
- 8 K. B. Narayanan and N. Sakthivel, *Adv. Colloid Interface Sci.*, 2011, **169**, 59.
- 9 N. Ahmad, S. Sharma, M. K. Alam, V. N. Singh, S. F. Shamsi, B. R. Mehta and A. Fatm, *Colloids Surf., B*, 2010, **81**, 81.
- 10 M. Sathishkumar, K. Sneha and Y. S. Yun, *Bioresour. Technol.*, 2010, **101**, 7958.
- 11 N. Muniyappan and N. S. Nagarajan, *Process Biochem.*, 2014, **49**, 1054.
- 12 C. Rajkuberan, K. Sudha, G. Sathishkumar and S. Sivaramakrishnan, *Spectrochim. Acta, Part A*, 2015, **136**, 924.
- 13 D. M. Parkin, F. Bray, J. Ferlay and P. Pisani, *Ca-Cancer J. Clin.*, 2005, **5**, 574.
- 14 F. Bray and B. Moller, *Nat. Rev. Cancer*, 2006, **6**, 63.
- 15 P. Parhi, C. Mohanty and S. K. Sahoo, *Drug Discovery*, 2012, **17**, 1044.
- 16 H. Yao, W. Xu, X. Shi and Z. Zhang, *J. Environ. Sci. Health, Part C: Environ. Carcinog. Ecotoxicol. Rev.*, 2011, **29**, 1.
- 17 E. R. Kasala, L. N. Bodduluru, R. M. Madana, K. V. Athira, R. Gogoi and C. C. Barua, *Toxicol. Lett.*, 2015, **233**, 214.
- 18 S. Chakraborty, S. Basu, A. Lahiri and S. Basak, *J. Mol. Struct.*, 2010, **977**, 180.
- 19 S. Dawar, N. Singh, R. K. Kanwar, R. L. Kennedy, R. N. Veedu, S. F. Zhou, S. Krishnakumar, S. Hazra, S. Sasidharan, W. Duan and J. R. Kanwar, *Drug Discovery Today*, 2013, **18**, 1292.
- 20 M. S. Bhojani, M. V. Dort, A. Rehemtulla and B. D. Ross, *Mol. Pharm.*, 2010, **7**, 1921.
- 21 Y. Q. Du, X. X. Yang, W. L. Li, J. Wang and C. Z. Huang, *RSC Adv.*, 2014, **4**, 34830.
- 22 X. Huang, I. H. E. Sayed, W. Qian and M. A. E. Sayed, *J. Am. Chem. Soc.*, 2006, **128**, 2115.
- 23 W. Cai, T. Gao, H. Hong and J. Sun, *Nanotechnol., Sci. Appl.*, 2008, **1**, 1.
- 24 D. K. Singh, R. Jagannathan, P. Khandelwal, P. M. Abraham and P. Poddar, *Nanoscale*, 2013, **5**, 1882.
- 25 L. David, B. Moldovan, A. Vulcu, L. Olenic, M. P. Schrepler, E. F. Fodor, A. Florea, M. Crisan, I. Chiorean, S. Clichici and G. A. Filip, *Colloids Surf., B*, 2014, **122**, 767.
- 26 K. Chaloupka, Y. Malam and A. M. Seifalian, *Trends Biotechnol.*, 2010, **28**, 580.
- 27 S. Mukherjee, D. Chowdhury, R. Kotcherlakota, S. Patra, B. Vinothkumar, M. P. Bhadra, B. Sreedhar and C. R. Patra, *Theranostics*, 2014, **4**, 316.
- 28 T. Mosmann, *J. Immunol. Methods*, 1983, **65**, 55.
- 29 S. K. Jaganathan, A. Mazumdar, D. Mondhe and M. Mandal, *Cell Biol. Int.*, 2011, **35**, 607.
- 30 P. Venkatesan, N. Puvvada, R. Dash, B. N. P. Kumar, D. Sarkar, B. Azab, A. Pathak, S. C. Kundu, P. B. Fisher and M. Mandal, *Biomaterials*, 2011, **32**, 3794.
- 31 J. J. Mock, M. Barbic, D. R. Smith, D. A. Schultz and S. Schultz, *J. Chem. Phys.*, 2002, **116**, 6755.
- 32 K. Kwon, K. Y. Lee, Y. W. Lee, M. Kim, J. Heo, S. J. Ahn and S. W. Han, *J. Phys. Chem. C*, 2007, **111**, 1161.
- 33 Q. Guo, Q. Guo, J. Yuan and J. Zeng, *Colloids Surf., A*, 2014, **441**, 127.
- 34 S. P. Dubey, M. Lahtinen and M. Sillanpaaa, *Process Biochem.*, 2010, **45**, 1065.
- 35 J. Y. Song and B. S. Kim, *Bioprocess Biosyst. Eng.*, 2009, **32**, 79.
- 36 A. Rai, A. Singh, A. Ahmad and M. Sastry, *Langmuir*, 2006, **22**, 736.
- 37 G. Sathishkumar, C. Gobinath, A. Wilson and S. Sivaramakrishnan, *Spectrochim. Acta, Part A*, 2014, **128**, 285.
- 38 Y. Zhou, W. Lin, J. Huang, W. Wang, Y. Gao, L. Lin, Q. Li, L. Lin and M. Du, *Nanoscale Res. Lett.*, 2010, **5**, 1351.
- 39 A. D. Dwivedi and K. Gopal, *Colloids Surf., A*, 2010, **369**, 27.
- 40 S. S. Shankar, A. Rai, A. Ahmad and M. Sastry, *J. Colloid Interface Sci.*, 2004, **275**, 496.
- 41 J. Kasthuri, S. Veerapandian and N. Rajendiran, *Colloids Surf., B*, 2009, **68**, 55.
- 42 S. Li, Y. Shen, A. Xie, X. Yu, L. Qiu, L. Zhang and Q. Zhang, *Green Chem.*, 2007, **9**, 852.
- 43 D. Philip, C. Unni, S. A. Aromal and V. K. Vidhu, *Spectrochim. Acta, Part A*, 2011, **78**, 899.
- 44 D. Philip, *Spectrochim. Acta, Part A*, 2009, **73**, 374.
- 45 C. Krishnaraj, E. G. Jagan, S. Rajasekar, P. Selvakumar, P. T. Kalaichelvan and N. Mohan, *Colloids Surf., B*, 2010, **76**, 50.
- 46 T. J. I. Edison and M. G. Sethuraman, *Process Biochem.*, 2012, **47**, 1351.
- 47 A. Nel, T. Xia, L. Madler and N. Li, *Science*, 2006, **311**, 622.
- 48 M. E. Selim and A. A. Hendi, *Asian Pac. J. Cancer Prev.*, 2012, **13**, 1617.
- 49 M. Jeyaraj, A. Renganathan, G. Sathishkumar, A. Ganapathi and K. Premkumar, *RSC Adv.*, 2015, **5**, 2159.
- 50 C. Greulich, J. Diendorf, T. Simon, G. Eggeler, M. Epple and M. Koller, *Acta Biomater.*, 2011, **7**, 347.
- 51 P. V. AshaRani, G. L. KahMun, M. P. Hande and S. Valiyaveettil, *ACS Nano*, 2009, **3**, 279.
- 52 M. Jeyaraj, M. Rajesh, R. Arunb, D. MubarakAli, G. Sathishkumar, G. Sivanandhan, G. K. Dev, M. Manickavasagam, K. Premkumar, N. Thajuddin and A. Ganapathi, *Colloids Surf., B*, 2013, **102**, 708–717.
- 53 M. Jeyaraj, R. Arun, G. Sathishkumar, D. MubarakAli, M. Rajesh, G. Sivanandhan, G. Kapildev, M. Manickavasagam, N. Thajuddin and A. Ganapathi, *Mater. Res. Bull.*, 2014, **52**, 15.
- 54 S. Kim, J. E. Choi, J. Choi, K. H. Chung, K. Park, J. Yie and D. Y. Ryu, *Toxicol. in Vitro*, 2009, **23**, 1076.
- 55 M. J. Piao, K. A. Kang, I. K. Lee, H. S. Kim, S. Kim, J. Y. Choi, J. Choi and J. W. Hyun, *Toxicol. Lett.*, 2011, **201**, 92.
- 56 S. Selvaraj, S. Krishnaswamy, V. Devashya, S. Sethuraman and U. M. Krishnan, *Langmuir*, 2011, **27**, 13374.
- 57 S. Ruden, K. Hilpert, M. Berditsch, P. Wadhwan and A. S. Ulrich, *Antimicrob. Agents Chemother.*, 2009, **53**, 3538.
- 58 K. P. Kumar, W. Paul and C. P. Sharma, *Process Biochem.*, 2011, **46**, 2007.